Title

Assessing the effects of forest biomass reductions on forest health and streamflow

Permalink

https://escholarship.org/uc/item/33p977kg

Journal

Hydrological Processes, 35(3)

ISSN

0885-6087

Authors

R., Ryan
Ray, Ram L
Conklin, Martha H
et al.

Publication Date

2021-03-01

DOI

10.1002/hyp.14114

Peer reviewed

Assessing the effects of forest biomass reductions on forest health and streamflow

Ryan R. Bart[1,a], Ram L. Ray[2], Martha H. Conklin[1], Mohammad Safeeq[3,4,5], Philip C. Saksa[6], Christina L. Tague[7], Roger C. Bales[1,4]

[1]Sierra Nevada Research Institute, University of California, Merced. [2]Cooperative Agricultural Research Center, College of Agriculture and Human Sciences, Prairie View A&M University, TX. [3]University of California, Division of Agriculture and Natural Resources, Davis. [4]Civil and Environmental Engineering, University of California, Merced. [5]Pacific Southwest Research Station, USDA Forest Service, Fresno, CA. [6]Blue Forest, Sacramento, CA. [7]Bren School of Environmental Science and Management, University of California, Santa Barbara. [a]Correspondence: rbart3@ucmerced.edu

Abstract. Forest biomass reductions in overgrown forests have the potential to provide hydrologic benefits in the form of improved forest health and increased streamflow production in water-limited systems. Biomass reductions may also alter evaporation. These changes are generated when water that previously would have been transpired or evaporated from the canopy of the removed vegetation is transferred to transpiration of the remaining vegetation, streamflow, and/or non-canopy evaporation. In this study, we combined a new vegetation-change water-balance approach with lumped hydrologic modeling outputs to examine the effects of forest biomass reductions on transpiration of the remaining vegetation and streamflow in California's Sierra Nevada. We found that on average, 102 mm and 263 mm (8.0% and 20.6% of mean annual precipitation [MAP]) of water were made available following 20% and 50% forest biomass-reduction scenarios, respectively. This water was then partitioned to both streamflow and transpiration of the remaining forest, but to varying degrees depending on post-biomass-reduction precipitation levels and forest biomass-reduction intensity. During dry periods, most of the water (approximately 200 mm [15.7% on MAP] for the 50% biomass-reduction scenario) was partitioned to transpiration of the remaining trees, while less than 50 mm (3.9% on MAP) was partitioned to streamflow. This increase in transpiration during dry periods would likely help trees maintain forest productivity and resistance to drought. During wet periods, the hydrologic benefits of forest biomass reductions shifted to streamflow (200 mm [15.7% on MAP]) and away from transpiration (less than 150 mm [11.8% on MAP]) as the remaining trees became less water stressed. We also found that streamflow benefits per unit of forest biomass reduction increased with biomass-reduction intensity, whereas transpiration benefits decreased. By accounting for changes in vegetation, the vegetation-change water balance developed in this study provided an improved assessment of watershed-scale forest health benefits associated with forest biomass reductions.

Keywords: biomass reduction, RHESSys, Sierra Nevada, streamflow, transpiration, snowpack

1. Introduction

When forest biomass (e.g., stems, branches, leaf area) is reduced, water that previously would have been transpired or evaporated from the canopy of the removed vegetation can be partitioned to other ecohydrologic processes, including transpiration of the remaining vegetation, streamflow, and non-canopy evaporation. In overgrown forests with water-limited vegetation, the former two changes can be beneficial. Lower forest biomass may reduce competition for water and increase transpiration amongst the remaining vegetation; increasing forest health and reducing vulnerability to drought and climate change (Sohn et al., 2016; Tague & Moritz, 2019; van Mantgem et al., 2020). Reductions in biomass may also decrease total forest water use, increasing the amount of water available for streamflow and downstream uses (Brown et al., 2005; Stednick, 1996). However, since both of these hydrologic benefits, as well as evaporation, rely on the same source of water made available from biomass reductions, water cannot be fully allocated to all three processes simultaneously (Bart et al., 2021). Yet despite the importance of quantifying the hydrologic benefits of biomass reductions, there is still uncertainty about how the water made available is partitioned to streamflow and transpiration of remaining vegetation (Tague et al., 2019).

Quantifying the partitioning of water made available from biomass reductions is challenging because the benefits in terms of increased vegetation transpiration and streamflow are frequently evaluated at different scales. Transpiration is generally quantified at the tree or stand scale. For example, Park et al. (2018) used sap-flow measurements to estimate an increase in tree transpiration following forest thinning, while Dore et al. (2012) used eddy-covariance measurements to estimate that stand evapotranspiration had only small, short-lived reductions following forest thinning. Post-reduction changes in streamflow, on the other hand, are an integrated watershed-scale measure. Numerous studies have examined streamflow response to biomass reductions such as fuel treatments, deforestation, and wildfire (Andréassian, 2004; Bosch & Hewlett, 1982; Brown et al., 2005; Stednick, 1996) and concluded that streamflow generally increases following biomass reductions. However, Goeking & Tarboton (2020) showed that for many non-stand replacing disturbances, streamflow may decrease. These decreases can occur as a consequence of increased regrowth transpiration (Bennett et al., 2018), sublimation (Harpold et al., 2014), or soil evaporation (Biederman et al., 2014) following biomass reductions.

Besides canopy evaporation, non-canopy evaporation processes (e.g., soil evaporation, litter

evaporation, sublimation) may also be altered by biomass reductions. Changes in evaporation after biomass reduction may act as either a source of additional water that can be partitioned to transpiration of the remaining vegetation and streamflow (Krogh et al., 2020), or as a sink where evaporation processes increase (Biederman et al., 2014). This latter pathway is often not considered to be a hydrologic benefit, but nonetheless must be understood in order to properly quantify potential streamflow and forest health benefits.

Few studies have simultaneously investigated how changes in the water balance following forest biomass reductions are partitioned to forest health benefits and streamflow benefits, despite the processes being intricately linked. An empirical study by Bart et al. (2021) found that fuel-treatments lessened drought mortality in some watersheds while increasing streamflow in other watersheds, a contrast that was attributed to differences in the partitioning of the water made available by fuel treatments. However, since assessing forest health and streamflow change empirically remains challenging, hydrologic modeling provides an alternative approach for evaluating changes in the partitioning of water made available from biomass reductions. Saksa et al. (2017) used a distributed ecohydrologic model to show that streamflow in wetter watersheds was more responsive to low-intensity thinning events than drier watersheds. The study also noted that watershed-scale transpiration decreased with fuel treatments, however, the study did not explicitly evaluate changes in forest water use of the remaining vegetation. This was partly due to a lack of lumped water-balance approaches for analyzing changes in transpiration for vegetation that remains after biomass reductions, as most water-balance approaches only assess changes in total watershed-scale transpiration.

In California, demands on streamflow for urban, agricultural, and environmental water needs frequently exceed supplies (Hanak et al., 2017). Meanwhile, forests in the Sierra Nevada, where many of the over-allocated rivers in the state originate (Grantham & Viers, 2014), have become overly dense due to historical policies of fire exclusion and are increasingly vulnerable to drought stress (Van Gunst et al., 2016). Thus, Sierra Nevada forests provide an important location for examining how forest biomass reductions may be able to offset one or both of these pressing needs in California.

In this study, we introduce a new vegetation-change water balance for quantifying the effect of forest biomass reductions on forest water use and streamflow at the lumped watershed scale. The approach requires only watershed-scale outputs of evaporation, transpiration, streamflow and change in storage, as well as an estimate of the percent vegetation change in the watershed. We demonstrate the utility of the water balance approach by applying it to watershed-level modeling outputs in three watersheds of the Kings River Experimental Watersheds (KREW) in the southern Sierra Nevada, California. The modeling design allowed us to address two research questions. First, how are the hydrologic benefits of reductions in forest biomass partitioned to transpiration of the remaining trees versus streamflow? Second, how do the hydrologic benefits vary with biomass-reduction intensity and precipitation level? These new insights will increase our understanding of how the restoration of overstocked forests affect hydrologic processes.

2. Methods

2.1. Providence watersheds. We examined the effects of forest biomass reduction on streamflow and transpiration in three Providence Creek sub-watersheds, P301, P303, and P304, located in the Southern Sierra Nevada (Figure 1). These watersheds are part of the KREW, a long-term ecological and streamflow monitoring site for headwater management research (Hunsaker et al., 2012), and the Southern Sierra Critical Zone Observatory (O'Geen et al., 2018). The drainage areas of the three watersheds range from 0.49 km² to 1.32 km² and mean elevations range from 1899 masl to 1979 masl with relief from 213 m to 318 m (Table 1). The watersheds have moderately steep slopes (19% to 22%) and are southwest facing. Drainage density ranges from 6.9 to 7.4 km/km². The parent material in the Providence watersheds is granite. Regolith thickness in P301 averages 1.5 m but is also highly variable, ranging from 0 m with exposed granite to over 10 m (O'Geen et al., 2018). The dominant soil in P301 is characterized as Gerle-Cagwin (soil depth 76-127 cm) and the dominant soil in P303 and P304 is Shaver (soil depth 102-203 cm) (Hunsaker et al., 2012).

Vegetation in Providence is largely made up of Sierran mixed-conifer forest with limited amounts of mixed chaparral and barren cover. Specific forest species include white fir (*Abies concolor*), ponderosa pine (*Pinus ponderosa*), Jeffrey pine (*Pinus jeffreyi*), sugar pine (*Pinus lambertiana*) and incense cedar (*Calocedrus decurrens*). Mixed chaparral species include greenleaf manzanita (*Arctostaphylos patula*) and mountain whitethorn (*Ceanothus cordulatus*). The trees in Providence are all secondary growth, as the watersheds were harvested some time prior to the establishment of the KREW (Lydersen et al., 2019). The historical fire regime in Providence was characterized as low severity with fire-return intervals between 5-20 years (Kilgore & Taylor, 1979; Scholl & Taylor, 2010). However, fire suppression in the Sierra Nevada over the past century have caused fire to be excluded from the area. Consequently, the watersheds prior to recent fuel treatments were characterized as being overly

dense, with density estimates of ~608 stems/ha and live tree basal area estimates of ~51 m²/ha, averaged over the three watersheds (Lydersen et al., 2019).

The Providence Creek watersheds have a Mediterranean-type climate, with most precipitation falling between late fall and early spring. Summers are typically very dry with negligible amounts of precipitation. Mean annual precipitation measured 1274 mm over the period from 2004 to 2014, though year-to-year precipitation totals were highly variable, ranging from 635 mm to 2172 mm. The mean-annual daily high temperature in Providence was 14.0°C and the mean-annual daily low temperature was 5.5°C. Winter temperatures, however, are often near freezing and Providence receives a mix of rain and snowfall (Hunsaker et al., 2012). Mean-annual streamflow for P301, P303, and P304 was 437, 291, and 442 mm, respectively, reflecting differences in hydrologic behavior between the watersheds. Notably, P304 has a much higher baseflow component compared to the other two watersheds, with a Baseflow Index (BFI) of 88% versus 72% and 74% in P301 and P303, respectively (Safeeq & Hunsaker, 2016). As such, a higher proportion of the streamflow in P304 occurs in the summer and fall. P301, on the other hand, has greater spring runoff than the other two watersheds (Safeeq & Hunsaker, 2016). For all the watersheds, discharge skews primarily to the winter during low snowfall years, whereas peak discharge occurs during the spring in high snowfall years.

2.2. Vegetation-change water balance. The management of water-limited forests requires understanding and quantifying fluxes associated with forest management, often at the watershed scale. The standard watershed-scale water balance assesses changes in hydrologic fluxes in and out of a watershed and is defined as:

$$P_w = T_w + E_w + Q_w + dS_w \qquad (1)$$

where P is precipitation (mm), T is transpiration (mm), E is evaporation, which encompasses evaporation and sublimation from both the ground and vegetation canopy (mm), Q is streamflow (mm), dS is the change in storage (mm), and subscript w designates the watershed scale. The water balance can be modified to evaluate differences in fluxes before and after a vegetation change event:

$$\Delta P_w = \Delta T_w + \Delta E_w + \Delta Q_w + \Delta(dS_w) \qquad (2)$$

where Δ is the difference between post-change and pre-change values of each water balance component. This vegetation-change water balance represents the standard approach for comparing a lumped hydrologic flux response to a step change in vegetation. However, by evaluating all flux changes at the watershed scale, the water balance does not account for the amount of vegetation that has been modified in the watershed nor does it address how water has been internally reallocated. A representation of the flux changes as a function of remaining vegetation may provide a better estimate of forest biomass-reduction effects on forest health.

The water balance in Equation 2 can be modified to focus on changes in transpiration for the remaining vegetation by separating ΔT_w and ΔE_w into two components, corresponding to changes in the fluxes from vegetation that is removed (ΔT_{rmv} and ΔE_{rmv}) and changes in fluxes from vegetation that remains in a watershed following biomass reduction (ΔT_{rmn} and ΔE_{rmn}):

$$\Delta P_w = (\Delta T_{rmv} + \Delta T_{rmn}) + (\Delta E_{rmv} + \Delta E_{rmn}) + \Delta Q_w + \Delta(dS_w) \qquad (3)$$

where subscript *rmv* signifies vegetation that is removed and subscript *rmn* signifies vegetation that remains in the watershed. The definition for removed and remaining vegetation depends on the scale. For example, removed vegetation may correspond to individual trees that are extracted during fuel treatments with the remaining vegetation corresponding to the undisturbed individuals. At smaller scales, removed vegetation may relate to the leaves and branches that are eliminated, while the remaining vegetation relates to the intact vegetation components. In Equation 3, changes in watershed streamflow (ΔQ_w) and change in storage ($\Delta(dS_w)$) could also be separated into removed and remaining components, but for this analysis, we have kept them as lumped watershed metrics.

By rearranging Equation 3 and in the absence of changes in precipitation ($\Delta P_w = 0$), we obtain a vegetation-change water balance that emphasizes the partitioning of water from the removed vegetation to the remaining vegetation:

$$-\Delta T_{rmv} - \Delta E_{rmv} = \Delta T_{rmn} + \Delta E_{rmn} + \Delta Q_w + \Delta(dS_w). \qquad (4)$$

The fluxes on the left side of the equation represent changes in water availability from the vegetation biomass that was removed. The fluxes and change in storage on the right side of the equation represent the balance; where the changes in water availability from the removed biomass is reallocated. The advantage of the vegetation-change water balance in Equation 4 compared to the standard vegetation-change water balance in Equation 2 is that it characterizes changes in transpiration for the remaining vegetation, which is expected to provide a better metric of vegetation health benefits.

2.3. RHESSys model. The vegetation-change water balance in Equation 4 works with watershed-scale outputs when the amount of vegetation change occurs at sub-watershed scales. Consequently, this approach may be applied to the outputs of lumped parsimonious models, as well as to more complex, spatially distributed hydrologic models when distributed

outputs are computationally prohibitive and outputs are limited to the watershed scale. In this study, we used a spatially distributed daily time-step model, Regional Hydro-Ecologic Simulation System (RHESSys), to evaluate water-balance responses to forest biomass reductions. However, only the watershed-level outputs from RHESSys were generated in order to make the results more generalizable.

RHESSys is designed to simulate hydrologic, carbon, and nitrogen cycling (Tague & Band, 2004). The model has been tested and applied in watersheds throughout the Sierra Nevada for investigating the vegetation and climate interactions on ecohydrologic processes (Bart et al., 2016; Godsey et al., 2014; Saksa et al., 2020; Son & Tague, 2019). RHESSys uses a hierarchical approach to partition a landscape into hydrologically nested units, with patches (i.e., vegetation stands) contained within hillslopes, climate zones, and watersheds. For each patch, multiple vegetation strata can be specified.

Hydrologic fluxes in RHESSys are modeled from the top of the canopy to groundwater. Rainfall and snowfall may be intercepted by the canopy and litter based on vegetation size and functional type. Snowpack accumulation (both ground and canopy) is based on precipitation phases of snow and rain that were input into the model separately. Snowmelt is based on a quasi-energy budget model. Subsurface storage is divided into rooting, unsaturated, saturated, and groundwater stores. Radiation in RHESSys is calculated based on latitude, aspect, and atmospheric variables using the MT-CLIM model (Running et al., 1987) and is attenuated through each canopy layer to the surface. Evaporation and transpiration are derived using Penman-Monteith (Monteith, 1965). A detailed summary of RHESSys (version 5.15) can be found in Supplemental Material.

Although RHESSys can be run as a fully coupled biogeochemical cycling, vegetation growth, and hydrology model; here we run only the hydrologic components of the model.

2.4. Model setup, calibration, validation, and scenarios. RHESSys was set up using a Light Detection and Ranging (LiDAR)-based Digital Elevation Model (DEM) product at 5-m spatial resolution to generate watershed, hillslope, and patch units (Table 1) (Harpold et al., 2014). Canopy-cover fraction and Leaf-Area Index (LAI) for each patch were also obtained from the LiDAR following Richardson et al. (2009). The soils in the model were based on a sandy loam and the vegetation layer was parameterized using the default conifer parameter set provided in the RHESSys parameter database (https://github.com/RHESSys/ParamDB). This parameter set simulates vegetation based on common traits for the conifer vegetation type.

RHESSys has a minimum forcing dataset requirement of daily precipitation, minimum temperature, and maximum temperature, each of which is adjusted in model at the zone level through lapse rate parameters. These data were obtained from two KREW meteorological stations (Hunsaker & Safeeq, 2018), one located near the upper part of P303 at 1984 masl and a second located between the P301 and P303 stream gauges at 1750 masl (Figure 1). To improve the timing of soil-water infiltration, snow and rain phases at a daily time step were inputted into the model separately using a binary process where precipitation was designated as a snow event if the acoustic depth sensors (Bales et al., 2018a) located at either meteorological station recorded an increase in snow depth; otherwise it was labeled a rain event.

To constrain RHESSys, we used a multi-step, multi-variable calibration process. The model was calibrated to present-day conditions within the watershed, not conditions after biomass reductions. The meteorological record extended from water year 2004 to 2014, with the water year defined as October 1 of the previous year to September 30 of the current year. The model was calibrated in P303 to streamflow and snowpack for the period from 2004 to 2008. This calibration period was split by water year type to account for differences in watershed behavior: average/wet water years (2004-06, 2008) and a very-dry water year (2007). The model was validated in P303 for water years 2009 to 2014 and these parameters were transferred to P301 and P304, which were subsequently evaluated over the full record, 2004 to 2014.

Calibration of RHESSys was separated into two components, both of which are summarized here with details provided in Supplemental Material. Six subsurface flow and soil-storage parameters were quantitatively calibrated to daily streamflow using a Monte Carlo approach with 500 random parameter sets (Table 2). The modeled streamflow was compared to observed data that were measured from dual Parshall Montana flumes in each of the watersheds (Hunsaker & Safeeq, 2017). Three additional parameters affecting snowmelt were calibrated to observed snow water equivalent (SWE) obtained from a snow pillow at the upper Providence meteorological station (Bales et al., 2018a) (Table 2).

Calibration and validation performance of the model was determined using Nash-Sutcliffe Efficiency (NSE) and Nash-Sutcliffe Efficiency of log-transformed data (NSE_log) (Nash & Sutcliffe, 1970). Overall, modeled daily streamflow showed good agreement (NSE > 0.8, NSE_log >= 0.75) with observed values for both the calibration and validation periods in the P303 watershed (Figure 2, Table 3). Modeled daily SWE also showed a good ability to replicate snowpack accumulation and ablation in P303, with NSE values of

0.92 for calibration and validation. After transferring the calibrated parameters to P301 and P304, we again observed good agreement between modeled streamflow and the observed streamflow, with NSE values of 0.82 obtained for the non-calibrated watersheds.

Three scenarios were conducted in each of the watersheds using identical meteorological data as input: a baseline scenario, a 20% low-intensity biomass-reduction scenario, and a 50% high-intensity biomass-reduction scenario. Biomass reductions were conducted homogeneously throughout the watershed and a proportional amount of carbon was removed from all aboveground vegetation stores, including leaf and stem stores, but with no change in canopy cover. This biomass-removal approach was designed to represent a natural watershed where lower biomass would reflect a longer-term steady state associated with repeated lower-intensity disturbance. The respective amount of biomass removed is thus distributed across the forest stand. Canopy cover was not altered because biomass removal in stands with relatively high levels of initial biomass and leaf area (e.g., leaf area greater than 10) was not expected to substantially alter long-term cover faction (Saksa et al., 2020).

Within RHESSys, a reduction in biomass and leaf area affects several processes. First, LAI is used to estimate leaf-scale shortwave radiation available for transpiration and then is used to scale leaf-level transpiration to forest stands or patches. Second, biomass reductions produce a decrease in mean canopy height for a given patch. This has implications for fluxes such as evaporation, since Penman-Monteith (Monteith, 1965) includes a variable for atmospheric resistance that is calculated as a function of vegetation height, potentially leading to a change in evapotranspiration due to changes in atmospheric resistance estimates. Last, changes in biomass and LAI affect the amount of radiation that reaches the snowpack. A reduction in LAI decreases shortwave attenuation through the canopy, which may increase snowmelt rates. However, reductions in biomass also decrease longwave radiation from the canopy, which may offset increases in shortwave radiation.

Vegetation was fixed (i.e., no growth) during the 11-year simulations so we could isolate the hydrologic effects of biomass reductions over a wide array of meteorological conditions. We have also included deep groundwater losses within the change in storage term ($\Delta(dS_w)$) due to uncertainty in the actual magnitude and partitioning of these two variables. To compare monthly differences between hydrologic processes at different precipitation levels, results from the simulations were grouped by dry (precipitation range 635 to 869 mm) water years (2007, 2013, 2014), average (precipitation range 945 to 1047 mm) water years (2004, 2008, 2009, 2012), and wet (precipitation range 1598 to 2172 mm) water years (2005, 2006, 2010, 2011) based on natural breaks within the precipitation record.

2.5. Separating transpiration and evaporation into removed and remaining vegetation components. The outputs from each of the biomass-reduction scenarios were used to compute the terms of the water-balances in Equation 1, 2, and 4. In this section, we show how ΔT_{rmv}, ΔE_{rmv}, ΔT_{rmn}, and ΔE_{rmn} in Equation 4 were calculated as a function of watershed-scale model outputs and an estimate of the amount of vegetation change in the watershed.

Transpiration changes for the removed vegetation (ΔT_{rmv}) were computed as:

$$\Delta T_{rmv} = T_{rmv\_post} - T_{rmv\_pre} \tag{5}$$
$$T_{rmv\_post} = 0 \tag{6}$$
$$T_{rmv\_pre} = T_{w\_pre} \times F_{veg} \tag{7}$$

where T_{rmv_post} is the amount of transpiration (in this case zero) associated with the removed vegetation following biomass reductions, T_{rmv_pre} is the amount of transpiration from the removed vegetation prior to biomass reductions, T_{w_pre} is the total watershed transpiration prior to biomass reductions, and F_{veg} is the fraction of total vegetation removed in the model. In equation 7, we assume a linear relation between amount of vegetation removed and the amount of transpiration change, though further work will be required to better specify this relation.

Estimating the change in evaporation following biomass reductions is more complicated than transpiration since evaporation may be an aggregation of multiple individual processes (e.g., canopy, litter, snowpack, and soil evaporation). As such, the calculation of evaporation changes for the removed vegetation (ΔE_{rmv}) involved a two-part process comprising canopy evaporation and non-canopy evaporation. It was assumed that changes in canopy evaporation, from both rain and snow, was the only evaporation component that could be directly calculated as a function of F_{veg}, and as such, was calculated in a similar manner to transpiration. Canopy evaporation changes for the removed vegetation (ΔE_canopy_{rmv}) were computed as:

$$\Delta E\_canopy_{rmv} = E\_canopy_{rmv\_post} - E\_canopy_{rmv\_pre} \tag{8}$$
$$E\_canopy_{rmv\_post} = 0 \tag{9}$$
$$E\_canopy_{rmv\_pre} = E_{w\_pre} \times F_{veg} \times F_E \tag{10a}$$
$$E\_canopy_{rmv\_pre} = E\_canopy_{w\_pre} \times F_{veg} \tag{10b}$$

where $E\_canopy_{rmv\_post}$ is the amount of canopy evaporation (in this case zero) associated with the removed vegetation following biomass reductions and $E\_canopy_{rmv\_pre}$ is the canopy evaporation from the removed vegetation prior to biomass reductions. $E\_canopy_{rmv\_pre}$ in Equation 10 may be computed

differently, depending on the modeling outputs available. If only watershed-scale outputs of total evaporation prior to biomass reductions (E_{w_pre}) are available, then $E\_canopy_{rmv\_pre}$ may be computed using Equation 10a with an estimate of the canopy evaporation fraction relative to total evaporation (F_E) in the watershed prior to biomass reductions. If watershed-scale outputs of total canopy evaporation prior to biomass reductions ($E\_canopy_{w\_pre}$) are available, as was the case of this study, then $E\_canopy_{rmv\_pre}$ may be computed using Equation 10b.

Changes in non-canopy evaporation components (e.g., litter, snowpack, and soil evaporation) could not be calculated in the same manner as canopy evaporation since there is uncertainty in how non-canopy processes respond to F_{veg}. Instead, changes in non-canopy evaporation for the removed vegetation ($\Delta E\_noncanopy_{rmv}$) were computed as:

$$\Delta E\_noncanopy_{rmv} = E\_noncanopy_{rmv\_post} - E\_noncanopy_{rmv\_pre} \qquad (11)$$

$$E\_noncanopy_{rmv\_pre} = \left(E_{w\_pre} - E\_canopy_{w\_pre}\right) \times F_{veg} \qquad (12)$$

$$E\_noncanopy_{rmv\_post} = E\_noncanopy_{rmv\_pre} \times \frac{E_{w\_post}}{E_{w\_pre} - E\_canopy_{rmv\_pre}} \qquad (13)$$

where $E\_noncanopy_{rmv\_post}$ is the amount of non-canopy evaporation associated with the removed vegetation following biomass reductions, $E\_noncanopy_{rmv\_pre}$ is the amount of non-canopy evaporation associated with the removed vegetation prior to biomass reductions, and E_{w_post} is the total watershed evaporation following biomass reductions. The ratio between E_{w_post} and the difference of $E\_canopy_{rmv\_pre}$ from E_{w_pre} in Equation 13 compares evaporation before and after biomass reductions for all non-$E\_canopy_{rmv\_pre}$ evaporation components. Since there was no canopy evaporation from the removed vegetation following biomass reductions (Equation 9), E_{w_post} in the numerator of the ratio represents the same processes as the denominator. Ratio values greater than or less than one represent modeled differences in pre- and post-biomass-reduction evaporation and Equation 13 allows these differences to be evenly distributed across all non-$E\_canopy_{rmv\_pre}$ evaporation components (i.e., litter, snowpack, and soil evaporation from the removed vegetation and canopy, litter, snowpack, and soil evaporation from the remaining vegetation). The total evaporation made available from biomass reductions (ΔE_{rmv}) was calculated by combining changes in canopy evaporation and changes in non-canopy evaporation:

$$\Delta E_{rmv} = \Delta E\_canopy_{rmv} + \Delta E\_noncanopy_{rmv}. \qquad (14)$$

Transpiration changes for the remaining vegetation (ΔT_{rmn}) were calculated as:

$$\Delta T_{rmn} = T_{rmn\_post} - T_{rmn\_pre} \qquad (15)$$

$$T_{rmn\_post} = T_{w\_post} - T_{rmv\_post} \qquad (16)$$

$$T_{rmn\_pre} = T_{w\_pre} \times (1 - F_{veg} \qquad (17)$$

where T_{rmn_post} is the amount of transpiration from the remaining vegetation following biomass reductions and T_{rmn_pre} is the amount of transpiration from the remaining vegetation prior to biomass reductions.

Evaporation changes for the remaining vegetation (ΔE_{rmn}) were calculated as:

$$\Delta E_{rmn} = E_{rmn\_post} - E_{rmn\_pre} \qquad (18)$$

$$E_{rmn\_pre} = E_{w\_pre} \times \left(1 - F_{veg}\right) \qquad (19)$$

$$E_{rmn\_post} = E_{rmn\_pre} \times \frac{E_{w\_post}}{E_{w\_pre} - E\_canopy_{rmv\_pre}} \qquad (20)$$

where E_{rmn_post} is the amount of evaporation from the remaining vegetation following biomass reductions and E_{rmn_pre} is the amount of evaporation from the remaining vegetation prior to biomass reductions.

3. Results

3.1. Annual. The annual water balance (Equation 1) for each Providence watershed shows precipitation partitioned to watershed-scale transpiration, evaporation, streamflow, and change in storage (Figure 3a, Table 4). Annual precipitation showed high variability from year to year, ranging from over 2000 mm in 2006 and 2011, to less than 750 mm in 2014. The largest flux out of each watershed was transpiration, which averaged 474±35 mm (37.2% of mean annual precipitation [MAP]) over all water years and watersheds. Transpiration was relatively stable from year to year and only began to decline in 2013 and 2014, during the beginning of the California drought. Evaporation was also fairly stable, averaging 154±11 mm, or ~¼ of total ET. Annual streamflow, on the other hand, was highly variable, averaging 390±111 mm (30.6% of MAP). As expected, high levels of streamflow were observed during wet water years, while little streamflow was observed during the driest years. Annual change in storage averaged 255±83 mm (20.0% of MAP) and was relatively high compared to streamflow in part because it includes both changes in watershed storage as well as deep groundwater directed out of the watershed as subsurface losses.

Changes in the annual water balance for the 20% and 50% biomass-reduction scenarios were proportionally similar to one another (Figure 3b and 3c, Table 4). For the 50% biomass-reduction scenario, biomass reductions reduced watershed-scale transpiration -56±19 mm (-4.4% of MAP) and evaporation -41±4 mm (-3.2% of MAP) over all water years and watersheds due to less biomass remaining in the watershed, while streamflow increased 86±23 mm (6.8% of MAP). For transpiration, the greatest decreases occurred during wet years. During dry years, the decreases in transpiration became either negligible or slightly increased. Offsetting the reductions in watershed transpiration and evaporation was streamflow, which increased with biomass reductions.

This increase was greatest during wet years, becoming negligible during dry years. The pattern for changes in storage was less definitive, as changes in storage both increased and decreased following biomass reductions depending on the watershed and year. Finally, we note that between the three Providence watersheds, the water balance and changes due to biomass reductions did not produce any meaningful differences in the interpretation of results. Due to this similarity in hydrologic functioning and the brevity of the results, we focus on the aggregate behavior of the Providence watersheds with some attention to representative individual watersheds.

Using the vegetation-change water balance in Equation 4, the results in Figure 4 indicate that the mean annual amount of water made available from forest biomass reductions was 102 mm (8.0% of MAP) for the 20% biomass-reduction scenario and 263 mm (20.6% of MAP) for the 50% biomass-reduction scenario. Most of this water was generated by reductions in transpiration from the removed vegetation (T_{rmv}), with smaller reductions in canopy evaporation (E_{rmv}) (Figure 4). Overall, 78% and 69% of the water made available from biomass reductions was partitioned to transpiration in the remaining trees (T_{rmn}) for the 20% and 50% scenarios, respectively (Table 4). Evaporation from remaining vegetation (E_{rmn}) slightly decreased following biomass reductions for all years (Figure 4). Changes in post-biomass-reduction streamflow and storage showed identical changes as those documented using Equation 2 and displayed in Figure 3, as these variables were unchanged in both equations.

We observed that the partitioning of water made available from forest biomass reductions varied with annual precipitation, with the greatest effects of precipitation variation associated with streamflow and transpiration in the remaining vegetation (Figure 5). The amount of water partitioned to transpiration in the remaining vegetation decreased with wetter conditions, from approximately 200 mm (15.7% of MAP) when precipitation was less than 1000 mm to less than 150 mm (11.8% of MAP) when precipitation was greater than 2000 mm for the 50% biomass-reduction scenario. This decrease occurred because the remaining trees had lower water stress during wet years and require less additional water to satisfy atmospheric demands. In contrast, the amount of water partitioned to streamflow increased with higher annual precipitation. Under dry conditions, the 50% biomass-reduction scenario increased streamflow by less than 50 mm (3.9% of MAP), but under wet conditions, the same amount of biomass reduction increased streamflow by nearly 200 mm (15.7% of MAP) (Figure 5). Hydrologic partitioning to evaporation of the remaining vegetation and change in storage showed little response to annual precipitation variability, with

a slightly negative relation for both variables (Figure 5).

We compared the proportional gain in transpiration of the remaining vegetation and streamflow for a given amount of biomass reduction at both the 20% and 50% biomass reduction levels in order to understand if the relative transpiration benefits to the remaining vegetation increased or decreased compared to streamflow for an incremental increase in biomass reduction (Figure 6). We found that the proportional gain in transpiration of the remaining vegetation was 3.9 versus 3.6 mm per 1% biomass reduced for the 20% and 50% biomass-reduction scenarios, respectively. On the other hand, the proportional gain in streamflow was 1.4 versus 1.7 mm per 1% biomass reduced for the respective scenarios. Each of these gains were statistically significant at p<0.01.

***3.2. Subannual**. The effect of precipitation levels on the partitioning of water made available from biomass reduction was examined on a monthly basis in P303 for the three driest, four average, and four wettest water years of the 50% biomass-reduction scenario (Figure 7). Biomass reductions increased transpiration in the remaining vegetation year-round during the dry and average water years, with the largest increases occurring during late spring and summer. During wet water years, the increase in transpiration in the remaining vegetation was similar to that of the dry and moderate water years from the middle of spring (May) through the fall (November). However, biomass reductions had little effect during the winter and generated a decrease in transpiration in the remaining vegetation during the early spring (March and April). Forest biomass reductions generated a small reduction in the evaporation of remaining vegetation during the wet season (November to May), with minimal changes observed during the dry season.

Biomass-reduction effects on the monthly water partitioning to streamflow differed with precipitation levels (Figure 7). During dry water years, forest biomass reductions produced minimal streamflow change throughout the year, with only a small increase during the spring (March to May). In contrast, biomass reductions during wet water years produced large increases in streamflow throughout the wet period (December to July), with the largest increases peaking during May. These were the periods when water demand for transpiration in the remaining vegetation was most satisfied and excess water could be partitioned to streamflow. The large increase in late-spring streamflow was also driven by an increase in snowmelt (Figure 8). During wet years, biomass reductions generated a larger snowpack compared to the baseline scenario, with a maximum increase of 62 mm (15%) for the 50% biomass-reduction scenario. Greater snowpack occurred following biomass

reductions in part because there was less canopy interception of snowfall and less longwave radiation emitted by vegetation, the latter which contributed to a 15 mm (45%) reduction in sublimation and a 34 mm (9%) reduction in snowmelt during the January to March winter period (Figure 8). During spring, however, the control on snowmelt transitioned as temperatures and shortwave radiation increased. A smaller LAI for the 50% biomass-reduction scenario produced less vegetation attenuation and greater radiation absorption by the snowpack. Consequently, spring snowmelt proceeded more rapidly, with snowpack depletion occurring 4 days earlier for the 50% biomass-reduction scenario compared to baseline conditions during wet years (Figure 8). When combined with the larger snowpack produced by biomass reductions during the winter, the rapid snowmelt generated much higher spring streamflow following biomass reductions, with May streamflow increasing by 66 mm (39%) for the 50% biomass-reduction scenario.

4. Discussion

4.1. Do reductions in biomass increase forest health, streamflow, or both? In this study, we have demonstrated that biomass reductions can increase both transpiration of the remaining vegetation, which we use as a surrogate for forest health in these seasonally water-limited watersheds, and streamflow, but do so to varying degrees depending on the biomass-reduction intensity and post-biomass-reduction precipitation levels. We found that on a mean-annual basis, 102 mm (8.0% of MAP) and 263 mm (20.6% of MAP) of water were made available following the 20% and 50% biomass-reduction scenarios, respectively. The largest proportion of this water was partitioned to transpiration in the remaining vegetation since forest vegetation often has first access to any additional water in the rooting zone. We also found that biomass reductions can increase water availability for streamflow, but the magnitude of this flux was much more variable than transpiration, with the greatest amounts occurring during wet years and during the spring and early summer wet season. This latter result was consistent with other studies in the Sierra Nevada that have found that greater streamflow responses to vegetation change in wetter watersheds (Saksa et al., 2017) or during wetter years (Bart et al., 2016).

Higher-intensity biomass reductions had a greater effect on streamflow and transpiration in the remaining vegetation than lower-intensity reductions. However, the results also showed that the proportional benefit per unit vegetation removed was influenced by the overall biomass-reduction intensity. The streamflow benefit from having an incrementally higher biomass-reduction intensity increased as the overall intensity of

the biomass reduction was larger, whereas the transpiration benefit decreased (Figure 6). This occurred because while more water becomes available with more intense biomass removal, less of this water can be transpired by the diminished amount of remaining vegetation as the vegetation reach their water-use capacity. Consequently, the amount of transpiration per unit vegetation change decreases. The opposite effect was observed with streamflow, as the additional water that was not transpired by the remaining vegetation was partitioned to streamflow at a higher proportion. This has implications for how forest-restoration projects are implemented. Forest-restoration projects generally have limited resources and forest health and streamflow benefits may be used to incentivize and guide the placement of treatments within a watershed (McCann et al., 2020). If one of the goals is to maximize water use by neighboring trees to improve forest health, low-intensity biomass reduction across many stands would optimize this benefit. On the other hand, if an objective of forest restoration is to increase streamflow, our results indicate that intensive biomass reductions will provide larger benefits.

The modeling results showed that streamflow and forest health benefits from biomass reduction varied depending on precipitation levels, both at an annual and subannual scale. During dry periods, the benefits from biomass reductions skewed toward transpiration of the remaining vegetation, as water generally has to move though the rooting zone before making its way to groundwater or streamflow, allowing vegetation first access to this water (Bales et al., 2018b). Water demand from vegetation and from downstream users of streamflow is often greatest during dry periods, when extensive forest water stress can lead to mortality and streamflow in water-limited regions may be insufficient to satisfy downstream needs (Allen et al., 2010; Hanak et al., 2017). The results of this study suggest that biomass reductions are likely to primarily benefit forest health during these dry periods. Annually, water made available from biomass reductions was mostly partitioned to transpiration during dry years (Figure 5). Subannually, this additional water was available for transpiration throughout the water year, including the dry summer season when forest water stress peaks (Figure 7). Streamflow, on the other hand, observed little change from biomass reductions during dry periods, suggesting that biomass reductions will not directly alleviate downstream water needs during severe droughts. Still, we caution that these results focus only on a snapshot in time. Changes in forest structure as vegetation regrows, as well as future disturbances, can have complex effects on water use (Tague & Moritz, 2019). Further study is needed to explore the evolution of the effects shown here with dynamic vegetation.

During wet periods, the hydrologic benefits of biomass reductions shifted from transpiration to streamflow as the water stress in the remaining vegetation was lessoned during wet periods. In the Providence watersheds, we found that the partitioning of water made available from biomass reductions to streamflow during the wettest year was over ten times that of the driest year (190 mm vs. 11 mm). Unfortunately, from a water resources standpoint, the years with the greatest increase in streamflow following biomass reductions coincided with the time periods when downstream demand for additional streamflow is usually the lowest. Wet periods in regions such as California are often characterized by high rainfall and flooding events (Dettinger et al., 2011). During these periods, increases in streamflow have the potential to exacerbate stress on outdated water storage infrastructure (Koskinas et al., 2019). However, in cases where sufficient downstream storage capacity is available, such as groundwater recharge (Kocis & Dahlke, 2017), the additional streamflow produced from biomass reductions may be available for future uses. We also observed that biomass reductions produce both a larger snowpack and a more rapid spring snowmelt during wet years. For the 50% biomass-reduction scenario, these changes contributed to a 39% increase in streamflow during peak snowmelt. This large increase in streamflow has implications for downstream channel capacity and flooding.

4.2. Application of vegetation-change water balance.
We have introduced a vegetation-change water balance (Equation 4) that focuses on how water made available from biomass reductions is partitioned to transpiration for the remaining vegetation, evaporation for the remaining vegetation, streamflow, and changes in storage. This differs from the standard vegetation-change water balance (Equation 2), which assesses watershed-scale transpiration and evaporation change after biomass reduction and does not directly account for changes in the amount of vegetation in the watershed. The difference between the two water balances is important for our interpretation of biomass-reduction effects. The standard water balance showed that watershed-scale transpiration decreased following biomass reductions (Figure 3), whereas the new water balance showed that transpiration in the remaining vegetation increased following biomass reductions (Figure 4). Both water balances provided unique information, however, the vegetation-change water balance in Equation 4 provided a more-direct evaluation of the forest health benefits associated with biomass reductions. The new water balance provides an alternative approach for investigating why streamflow may not always change or sometimes decreases after biomass reductions (Goeking & Tarboton, 2020) by highlighting when water is preferentially used by the remaining vegetation and thereby not contributing to streamflow. The water balance may also be adapted for use at other scales, as well as for increases in vegetation biomass such as regrowth following disturbance.

4.3. Water balance and model uncertainties.
Model results must be interpreted in light of key assumptions and uncertainties. The vegetation-change water balance in Equation 4 showed that evaporation for the remaining vegetation decreased after biomass reductions (Figure 4). This result occurred in part due to the representation of biomass reductions in the model. In our biomass-reduction scenarios, biomass and LAI were reduced but canopy cover was not altered, representing biomass reductions for a natural watershed with repeated lower-intensity disturbance. These scenarios produced decreases in longwave radiation, decreases in shortwave attenuation through the canopy, and decreases in canopy interception, but did not increase exposed gaps that might occur under other biomass-reduction scenarios such as forest fuel treatments. In the Sierra Nevada, an increase in small gaps between canopies has been shown to increase snowpack accumulation since less snow is intercepted by the vegetation canopy but the snowpack is still partially shaded (Broxton et al., 2015; Stevens, 2017). Although snowpack sublimation may increase in canopy gaps, Harpold et al. (2020) found that this increase in sublimation did not offset decreases in canopy evaporation, generating more snowmelt. Thus, biomass reductions that contain canopy gaps may be expected to make more water available that can subsequently be partitioned to transpiration or streamflow. Nevertheless, because vegetation regrowth can rapidly fill in canopy cover gaps, the biomass reductions implemented in this study may better represent the long-term hydrological effects of biomass reductions.

One of the assumptions in the model was that following biomass reductions, the remaining vegetation would have access to all of the water made available. However, this assumption may overstate the amount of water that is partitioned to transpiration of the remaining vegetation if rooting systems are less developed and widespread under conditions when biomass is reduced compared to pre-reduction conditions. Further, forest-fuel treatments are often spatially concentrated, such that water made available in the treated areas may not be accessible by the remaining vegetation. In both cases, the extra water would then be partitioned to evaporation or streamflow.

RHESSys was calibrated to baseline conditions and not directly to biomass reductions, since no data existed for 20% and 50% biomass reductions at these sites. This lack of representative data after biomass reductions increased uncertainty in the study results as

an implicit assumption of the model was that the hydrologic behavior of the watershed was the same before and after biomass reductions.

Finally, there is a need for more empirical analyses of the partitioning of water to transpiration in the remaining vegetation and streamflow to corroborate the findings in this study. This will necessitate instrumentation to simultaneously measure evaporation, transpiration, and streamflow. At the watershed scale, assessment of biomass reduction benefits has generally been limited to streamflow, as this component of the water balance can be measured directly via a stream gauge, or more recently, indirectly by scaling ET measurements from eddy covariance towers with remote sensing and back calculating streamflow based on the water balance (Goulden & Bales, 2014). New combinations of techniques to quantify and scale evaporation and transpiration (Stoy et al., 2019), such as with sap flow sensors and eddy covariance, are needed to readily evaluate forest health benefits alongside streamflow benefits.

5. Summary

In this study, we simulated forest biomass reductions in three watersheds in the southern Sierra Nevada and analyzed the watershed-scale outputs using a new vegetation-change water balance. The water-balance approach allowed us to calculate changes in transpiration for the remaining vegetation and streamflow within the watershed. We found that although total transpiration in the watersheds decreased, transpiration for the remaining vegetation and streamflow both increased following biomass reductions. Transpiration increases in the remaining vegetation were highest under dry conditions and decreased with wetter conditions, as the remaining vegetation required less additional water due to lower water stress. Streamflow change following biomass reductions was minimal during dry conditions but increased substantially during wet conditions. Biomass-reduction intensity affected the partitioning of water to transpiration of the remaining vegetation and streamflow. High-intensity biomass reductions produced proportionally higher per unit increases in streamflow and lower per unit increases in transpiration in the remaining vegetation than low-intensity biomass reductions. The findings highlight the importance of evaluating biomass-reduction effects on transpiration of the remaining vegetation in combination with streamflow, as the hydrologic responses of both are intricately linked. These findings are also likely to be applicable outside the southern Sierra Nevada region, particularly for seasonally water-limited vegetation.

Data availability statement.

Data sources used as inputs to RHESSys are listed in the text. Outputs from RHESSys and the code used to analyze the data are openly available at https://doi.org/10.5281/zenodo.3959730.

References

Allen, C. D., Macalady, A. K., Chenchouni, H., Bachelet, D., McDowell, N., Vennetier, M., Kitzberger, T., Rigling, A., Breshears, D. D., Hogg, E. H. (Ted), Gonzalez, P., Fensham, R., Zhang, Z., Castro, J., Demidova, N., Lim, J.-H., Allard, G., Running, S. W., Semerci, A., & Cobb, N. (2010). A global overview of drought and heat-induced tree mortality reveals emerging climate change risks for forests. *Forest Ecology and Management*, *259*(4), 660–684. https://doi.org/10.1016/j.foreco.2009.09.001

Andréassian, V. (2004). Waters and forests: From historical controversy to scientific debate. *Journal of Hydrology*, *291*(1–2), 1–27. https://doi.org/10.1016/j.jhydrol.2003.12.015

Bales, R. C., Goulden, M. L., Hunsaker, C. T., Conklin, M. H., Hartsough, P. C., O'Geen, A. T., Hopmans, J. W., & Safeeq, M. (2018b). Mechanisms controlling the impact of multi-year drought on mountain hydrology. *Scientific Reports*, *8*(1), 690. https://doi.org/10.1038/s41598-017-19007-0

Bales, R., Stacy, E., Safeeq, M., Meng, X., Meadows, M., Oroza, C., Conklin, M., Glaser, S., & Wagenbrenner, J. (2018a). Spatially distributed water-balance and meteorological data from the rain–snow transition, southern Sierra Nevada, California. *Earth System Science Data*, *10*(4), 1795–1805. https://doi.org/10.5194/essd-10-1795-2018

Bart, R. R., Safeeq, M., Wagenbrenner, J. W., & Hunsaker, C. T. (2021). Do fuel treatments decrease forest mortality or increase streamflow? A case study from the Sierra Nevada (USA). *Ecohydrology*, *14*(1), e2254. https://doi.org/10.1002/eco.2254

Bart, R. R., Tague, C. L., & Moritz, M. A. (2016). Effect of tree-to-shrub type conversion in lower montane forests of the Sierra Nevada (USA) on streamflow. *PLOS ONE*, *11*(8), e0161805. https://doi.org/10.1371/journal.pone.0161805

Bennett, K. E., Bohn, T. J., Solander, K., McDowell, N. G., Xu, C., Vivoni, E., & Middleton, R. S. (2018). Climate-driven disturbances in the San Juan River sub-basin of the Colorado River. *Hydrology and Earth System Sciences*, *22*(1), 709–725. https://doi.org/10.5194/hess-22-709-2018

Biederman, J. A., Harpold, A. A., Gochis, D. J., Ewers, B. E., Reed, D. E., Papuga, S. A., & Brooks, P. D. (2014). Increased evaporation following widespread tree mortality limits streamflow response. *Water Resources Research*, *50*(7), 5395–5409. https://doi.org/10.1002/2013WR014994

Bosch, J. M., & Hewlett, J. D. (1982). A review of catchment experiments to determine the effect of vegetation changes on water yield and evapotranspiration. *Journal of Hydrology*, *55*(1–4), 3–23. https://doi.org/10.1016/0022-1694(82)90117-2

Brown, A. E., Zhang, L., McMahon, T. A., Western, A. W., & Vertessy, R. A. (2005). A review of paired catchment studies

for determining changes in water yield resulting from alterations in vegetation. *Journal of Hydrology*, *310*(1–4), 28–61. https://doi.org/10.1016/j.jhydrol.2004.12.010

Broxton, P. D., Harpold, A. A., Biederman, J. A., Troch, P. A., Molotch, N. P., & Brooks, P. D. (2015). Quantifying the effects of vegetation structure on snow accumulation and ablation in mixed-conifer forests. *Ecohydrology*, *8*(6), 1073–1094. https://doi.org/10.1002/eco.1565

Dettinger, M. D., Ralph, F. M., Das, T., Neiman, P. J., & Cayan, D. R. (2011). Atmospheric Rivers, Floods and the Water Resources of California. *Water*, *3*(2), 445–478. https://doi.org/10.3390/w3020445

Dore, S., Montes-Helu, M., Hart, S. C., Hungate, B. A., Koch, G. W., Moon, J. B., Finkral, A. J., & Kolb, T. E. (2012). Recovery of ponderosa pine ecosystem carbon and water fluxes from thinning and stand-replacing fire. *Global Change Biology*, *18*(10), 3171–3185. https://doi.org/10.1111/j.1365-2486.2012.02775.x

Godsey, S. E., Kirchner, J. W., & Tague, C. L. (2014). Effects of changes in winter snowpacks on summer low flows: Case studies in the Sierra Nevada, California, USA. *Hydrological Processes*, *28*(19), 5048–5064. https://doi.org/10.1002/hyp.9943

Goeking, S. A., & Tarboton, D. G. (2020). Forests and Water Yield: A Synthesis of Disturbance Effects on Streamflow and Snowpack in Western Coniferous Forests. *Journal of Forestry*, *118*(2), 172–192. https://doi.org/10.1093/jofore/fvz069

Goulden, M. L., & Bales, R. C. (2014). Mountain runoff vulnerability to increased evapotranspiration with vegetation expansion. *Proceedings of the National Academy of Sciences*, *111*(39), 14071–14075. https://doi.org/10.1073/pnas.1319316111

Grantham, T. E., & Viers, J. H. (2014). 100 years of California's water rights system: Patterns, trends and uncertainty. *Environmental Research Letters*, *9*(8), 084012. https://doi.org/10.1088/1748-9326/9/8/084012

Hanak, E., Lund, J., Arnold, B., Escriva-Bou, A., Gray, B., Green, S., Harter, T., Howitt, R., MacEwan, D., Medellín-Azuara, J., Moyle, P., & Seavy, N. (2017). *Water Stress and a Changing San Joaquin Valley* (p. 50). Public Policy Institute of California. http://www.ppic.org/main/publication.asp?i=1224

Harpold, A. A., Guo, Q., Molotch, N., Brooks, P. D., Bales, R., Fernandez-Diaz, J. C., Musselman, K. N., Swetnam, T. L., Kirchner, P., Meadows, M. W., Flanagan, J., & Lucas, R. (2014). LiDAR-derived snowpack data sets from mixed conifer forests across the Western United States. *Water Resources Research*, *50*(3), 2749–2755. https://doi.org/10.1002/2013WR013935

Harpold, Adrian A., Biederman, J. A., Condon, K., Merino, M., Korgaonkar, Y., Nan, T., Sloat, L. L., Ross, M., & Brooks, P. D. (2014). Changes in snow accumulation and ablation following the Las Conchas Forest Fire, New Mexico, USA. *Ecohydrology*, *7*(2), 440–452. https://doi.org/10.1002/eco.1363

Harpold, Adrian A., Krogh, S. A., Kohler, M., Eckberg, D., Greenberg, J., Sterle, G., & Broxton, P. D. (2020). Increasing the efficacy of forest thinning for snow using high-resolution modeling: A proof of concept in the Lake Tahoe Basin, California, USA. *Ecohydrology*, *13*(4), e2203. https://doi.org/10.1002/eco.2203

Hunsaker, C. T., & Safeeq, M. (2017). *Kings River Experimental Watersheds stream discharge* [Fort Collins, CO: Forest Service Research Data Archive.]. https://doi.org/10.2737/RDS-2017-0037

Hunsaker, C. T., & Safeeq, M. (2018). *Kings River Experimental Watersheds meteorology data* [Fort Collins, CO: Forest Service Research Data Archive.]. https://doi.org/10.2737/RDS-2018-0028

Hunsaker, C. T., Whitaker, T. W., & Bales, R. C. (2012). Snowmelt Runoff and Water Yield Along Elevation and Temperature Gradients in California's Southern Sierra Nevada. *JAWRA Journal of the American Water Resources Association*, *48*(4), 667–678. https://doi.org/10.1111/j.1752-1688.2012.00641.x

Kilgore, B. M., & Taylor, D. (1979). Fire History of a Sequoia-Mixed Conifer Forest. *Ecology*, *60*(1), 129–142. https://doi.org/10.2307/1936475

Kocis, T. N., & Dahlke, H. E. (2017). Availability of high-magnitude streamflow for groundwater banking in the Central Valley, California. *Environmental Research Letters*, *12*(8), 084009. https://doi.org/10.1088/1748-9326/aa7b1b

Koskinas, A., Tegos, A., Tsira, P., Dimitriadis, P., Iliopoulou, T., Papanicolaou, P., Koutsoyiannis, D., & Williamson, T. (2019). Insights into the Oroville Dam 2017 Spillway Incident. *Geosciences*, *9*(1), 37. https://doi.org/10.3390/geosciences9010037

Krogh, S. A., Broxton, P. D., Manley, P. N., & Harpold, A. A. (2020). Using Process Based Snow Modeling and Lidar to Predict the Effects of Forest Thinning on the Northern Sierra Nevada Snowpack. *Frontiers in Forests and Global Change*, *3*, 21. https://doi.org/10.3389/ffgc.2020.00021

Lydersen, J. M., Collins, B. M., & Hunsaker, C. T. (2019). Implementation constraints limit benefits of restoration treatments in mixed-conifer forests. *International Journal of Wildland Fire*, *28*(7), 495–511. https://doi.org/10.1071/WF18141

McCann, H., Butsic, V., Battles, J., Cisneros, R., Jin, Y., Kocher, S., Potts, M. D., & Stephens, S. (2020). *The Benefits of Headwater Forest Management, Technical Appendix: Review of the Scientific Literature* (p. 23). Public Policy Institute of California.

Monteith, J. L. (1965). Evaporation and environment. *Symp. Soc. Exp. Biol*, *19*, 205–234.

Nash, J. E., & Sutcliffe, J. V. (1970). River flow forecasting through conceptual models part I–A discussion of principles. *Journal of Hydrology*, *10*(3), 282–290.

O'Geen, A. (Toby), Safeeq, M., Wagenbrenner, J., Stacy, E., Hartsough, P., Devine, S., Tian, Z., Ferrell, R., Goulden, M., Hopmans, J. W., & Bales, R. (2018). Southern Sierra Critical Zone Observatory and Kings River Experimental Watersheds: A Synthesis of Measurements, New Insights, and Future Directions. *Vadose Zone Journal*, *17*(1). 1-18. https://doi.org/10.2136/vzj2018.04.0081

Park, J., Kim, T., Moon, M., Cho, S., Ryu, D., & Seok Kim, H. (2018). Effects of thinning intensities on tree water use, growth, and resultant water use efficiency of 50-year-old Pinus koraiensis forest over four years. *Forest Ecology and Management*, *408*, 121–128. https://doi.org/10.1016/j.foreco.2017.09.031

Richardson, J. J., Moskal, L. M., & Kim, S.-H. (2009). Modeling approaches to estimate effective leaf area index from aerial discrete-return LIDAR. *Agricultural and Forest Meteorology*, *149*(6), 1152–1160. https://doi.org/10.1016/j.agrformet.2009.02.007

Running, S. W., Nemani, R. R., & Hungerford, R. D. (1987). Extrapolation of synoptic meteorological data in mountainous terrain and its use for simulating forest evapotranspiration and photosynthesis. *Canadian Journal of Forest Research*, *17*(6), 472–483. https://doi.org/10.1139/x87-081

Safeeq, M., & Hunsaker, C. T. (2016). Characterizing Runoff and Water Yield for Headwater Catchments in the Southern Sierra Nevada. *Journal of the American Water Resources Association (JAWRA)*, *52*(6), 1327–1346. https://doi.org/10.1111/1752-1688.12457

Saksa, P.C., Conklin, M. H., Battles, J. J., Tague, C. L., & Bales, R. C. (2017). Forest thinning impacts on the water balance of Sierra Nevada mixed-conifer headwater basins. *Water Resources Research*, *53*(7), 5364–5381. https://doi.org/10.1002/2016WR019240

Saksa, Philip C., Bales, R. C., Tague, C. L., Battles, J. J., Tobin, B. W., & Conklin, M. H. (2020). Fuels treatment and wildfire effects on runoff from Sierra Nevada mixed-conifer forests. *Ecohydrology*, *13*(3), e2151. https://doi.org/10.1002/eco.2151

Scholl, A. E., & Taylor, A. H. (2010). Fire regimes, forest change, and self-organization in an old-growth mixed-conifer forest, Yosemite National Park, USA. *Ecological Applications*, *20*(2), 362–380. https://doi.org/10.1890/08-2324.1

Sohn, J. A., Saha, S., & Bauhus, J. (2016). Potential of forest thinning to mitigate drought stress: A meta-analysis. *Forest Ecology and Management*, *380*, 261–273. https://doi.org/10.1016/j.foreco.2016.07.046

Son, K., & Tague, C. (2019). Hydrologic responses to climate warming for a snow-dominated watershed and a transient snow watershed in the California Sierra. *Ecohydrology*, *12*(1), e2053. https://doi.org/10.1002/eco.2053

Stednick, J. D. (1996). Monitoring the effects of timber harvest on annual water yield. *Journal of Hydrology*, *176*(1–4), 79–95. https://doi.org/10.1016/0022-1694(95)02780-7

Stevens, J. T. (2017). Scale-dependent effects of post-fire canopy cover on snowpack depth in montane coniferous forests. *Ecological Applications*, *27*(6), 1888–1900. https://doi.org/10.1002/eap.1575

Stoy, P. C., El-Madany, T. S., Fisher, J. B., Gentine, P., Gerken, T., Good, S. P., Klosterhalfen, A., Liu, S., Miralles, D. G., Perez-Priego, O., Rigden, A. J., Skaggs, T. H., Wohlfahrt, G., Anderson, R. G., Coenders-Gerrits, A. M. J., Jung, M., Maes, W. H., Mammarella, I., Mauder, M., … Wolf, S. (2019). Reviews and syntheses: Turning the challenges of partitioning ecosystem evaporation and transpiration into opportunities. *Biogeosciences*, *16*(19), 3747–3775. https://doi.org/10.5194/bg-16-3747-2019

Tague, C. L., & Band, L. E. (2004). RHESSys: Regional Hydro-Ecologic Simulation System—An Object-Oriented Approach to Spatially Distributed Modeling of Carbon, Water, and Nutrient Cycling. *Earth Interactions*, *8*(19), 1–42. https://doi.org/10.1175/1087-3562(2004)8<1:RRHSSO>2.0.CO;2

Tague, Christina L., & Moritz, M. A. (2019). Plant Accessible Water Storage Capacity and Tree-Scale Root Interactions Determine How Forest Density Reductions Alter Forest Water Use and Productivity. *Frontiers in Forests and Global Change*, *2*(36). https://doi.org/10.3389/ffgc.2019.00036

Tague, Christina L., Moritz, M., & Hanan, E. (2019). The changing water cycle: The eco-hydrologic impacts of forest density reduction in Mediterranean (seasonally dry) regions. *WIREs Water*, *6*(4), e1350. https://doi.org/10.1002/wat2.1350

Van Gunst, K. J., Weisberg, P. J., Yang, J., & Fan, Y. (2016). Do denser forests have greater risk of tree mortality: A remote sensing analysis of density-dependent forest mortality. *Forest Ecology and Management*, *359*, 19–32. https://doi.org/10.1016/j.foreco.2015.09.032

van Mantgem, P. J., Kerhoulas, L. P., Sherriff, R. L., & Wenderott, Z. J. (2020). Tree-Ring Evidence of Forest Management Moderating Drought Responses: Implications for Dry, Coniferous Forests in the Southwestern United States. *Frontiers in Forests and Global Change*, *3*, 41. https://doi.org/10.3389/ffgc.2020.00041

Table 1: Watershed characteristics (modified from Safeeq and Hunsaker (2016)) and model setup details.

Characteristic	P301	P303	P304
Area (ha)	99	132	49
Mean elevation (masl)	1979	1905	1899
Relief (m)	318	292	213
Mean aspect (degrees)	208	233	249
Mean slope (%)	19	20	22
Drainage density (km/km^2)	7.4	7.4	6.9
Mean annual streamflow (mm)	437	291	442
Number of modeled hillslopes	791	571	268
Mean hillslope size (m^2)	1254	2318	1819
Number of modeled patches	9571	18617	8586
Mean patch size (m^2)	104	71	57

Aspect: north = 0 degrees

Table 2: Calibrated parameter values and initial parameter ranges for RHESSys.

Parameter	Description	P301	P303	P304	Initial Parameter Ranges
m (wet)	Decay of hydraulic conductivity with depth (m^{-1})	0.18	0.18	0.18	0.01 - 5
m (dry)	Decay of hydraulic conductivity with depth (m^{-1})	0.12	0.12	0.12	0.01 - 5
k	Saturated hydraulic conductivity (m d^{-1})	4.5	4.5	4.5	1 - 200
gw1	Groundwater bypass flow (%)	0.05-0.35	0.05-0.35	0.23-0.45	0 - 0.5
gw2	Groundwater drainage rate (%)	0	0	0.00005-0.0001	0 - 0.2
po (wet)	Pore size index (-)	0.3855	0.3855	0.3855	0.05 - 2
po (dry)	Pore size index (-)	0.2455	0.2455	0.2455	0.05 - 2
pa	Soil air entry pressure (m)	0.528	0.528	0.528	0.05 - 10
SLA	Specific leaf area (-)	8	8	8	5 - 20
SMTc (wet)	Snow melt temperature coefficient (m C^{-1})	0.0004	0.0004	0.0004	0.00001 - 0.001
SMTc (dry)	Snow melt temperature coefficient (m C^{-1})	0.0001	0.0001	0.0001	0.00001 - 0.001
β_{Mrad} (wet)	Radiation melt coefficient (m kJ^{-1} m^2 d^{-1})	0	0	0	0 - 0.5
β_{Mrad} (dry)	Radiation melt coefficient (m kJ^{-1} m^2 d^{-1})	0.4	0.4	0.4	0 - 0.5

Table 3: Model calibration and validation results.

Watershed	Variable	Objective Function	Calibration Period (2004-2008)	Validation Period (2009-2014)	Full Record (2004-2014)
P303	Streamflow	NSE	0.84	0.75	0.81
		NSE log	0.87	0.85	0.86
	Snow	NSE	0.92	0.92	0.92
P301	Streamflow	NSE	-	-	0.82
P304	Streamflow	NSE	-	-	0.82

Note: NSE = Nash-Sutcliffe Efficiency

Table 4: Mean annual water balance values (by water year) for the baseline and 50% biomass-reduction scenarios, averaged across all watersheds.

Scenario	Water balance component	Mean annual value and 95% CI (mm)	Mean annual value and 95% CI (% of MAP)
Baseline: Equation 1	Transpiration (T_w)	474 ± 35	37.2% ± 2.75%
	Evaporation (E_w)	154 ± 11	12.1% ± 0.86%
	Streamflow (Q_w)	390 ± 111	30.6% ± 8.71%
	Change in storage (dS_w)	255 ± 83	20% ± 6.51%
Change from baseline: Equation 2	Transpiration (ΔT_w)	-56 ± 19	-4.4% ± 1.49%
	Evaporation (ΔE_w)	-41 ± 4	-3.2% ± 0.31%
	Streamflow (ΔQ_w)	86 ± 23	6.8% ± 1.81%
	Change in storage ($\Delta(dS_w)$)	11 ± 5	0.9% ± 0.39%
Change from baseline: Equation 4	Transpiration (ΔT_{rmn})	181 ± 17	14.2% ± 1.33%
	Evaporation (ΔE_{rmn})	-15 ± 2	-1.2% ± 0.16%
	Streamflow (ΔQ_w)	86 ± 23	6.8% ± 1.81%
	Change in storage ($\Delta(dS_w)$)	11 ± 5	0.9% ± 0.39%

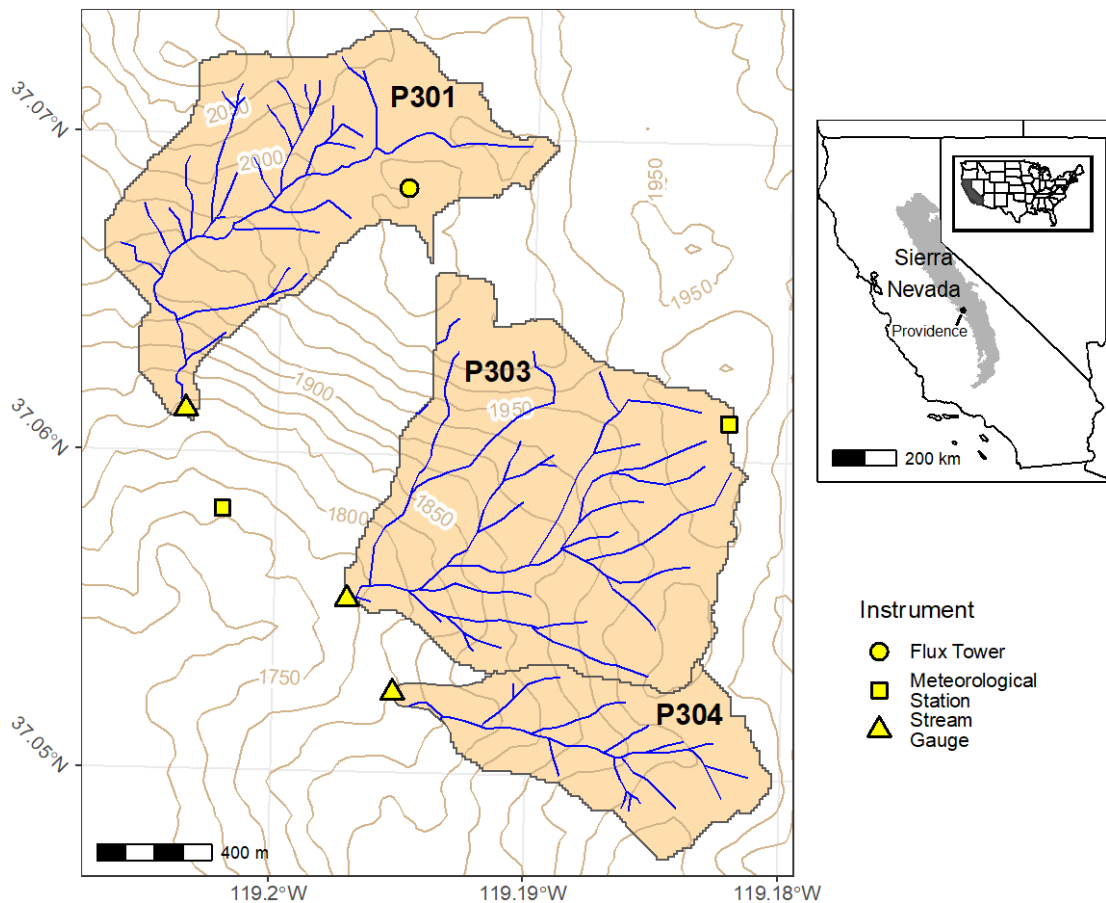CI: Confidence interval, MAP: Mean annual precipitation

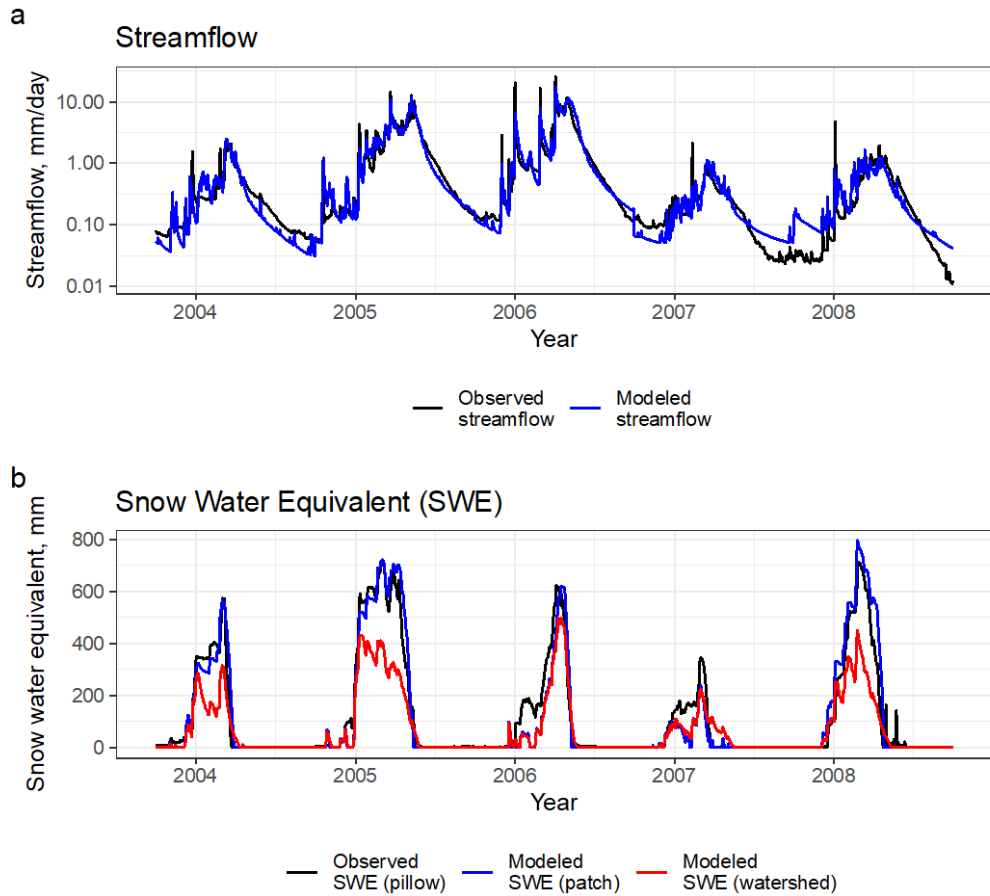**Figure 1: Map of Providence watersheds. Elevation contours are in masl.**

Figure 2: RHESSys calibration time-series for water years 2004 to 2008. a) Comparison of observed and modeled streamflow for P303 watershed. b) Comparison of observed snow water equivalent (SWE) at the upper Providence meteorological station, modeled SWE at the patch corresponding to the upper Providence meteorological station, and averaged modeled SWE over the P303 watershed.
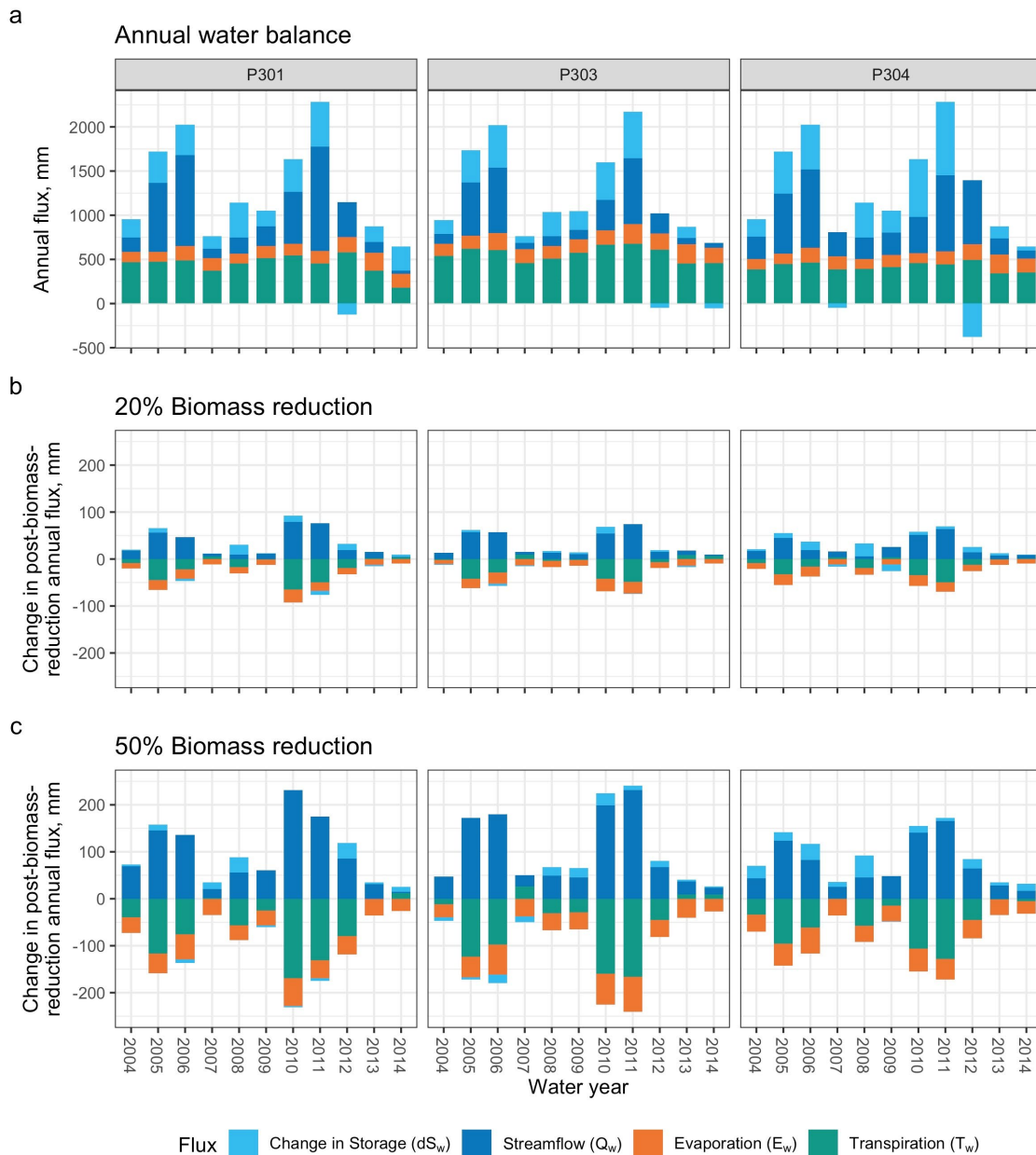
Figure 3: a) Watershed-scale annual water balance for the Providence watersheds showing transpiration, evaporation, streamflow, and change in storage (Equation 1). Precipitation is equal to the cumulative height of the bar above the zero line minus the cumulative height of the bar below the zero line. b) Change in post-biomass-reduction annual fluxes relative to baseline for the 20% biomass-reduction scenario (Equation 2). c) Change in post-biomass-reduction annual fluxes relative to baseline for the 50% biomass-reduction scenario (Equation 2). Water balances are by water year for all panels.

Figure 4: Amount and source of annual water made available from biomass reductions (left bar) and the partitioning of that water (right bar) for each water year averaged over all watersheds for the 20% and 50% biomass-reduction scenarios. The total change in the left bar is equal to the total change in the right bar.
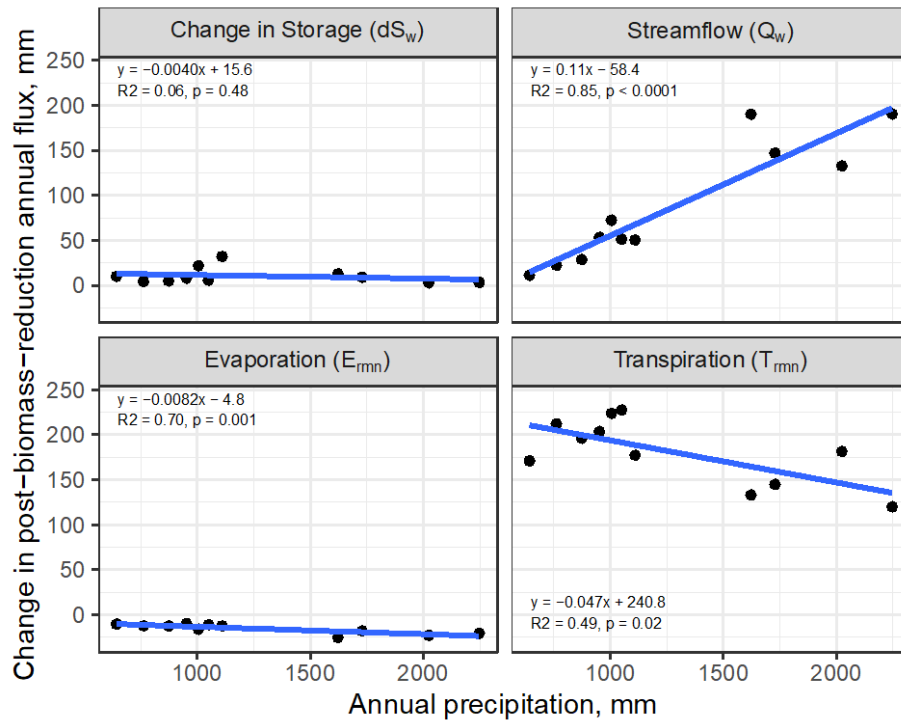
Figure 5: Relation between annual precipitation (mm) and post-biomass reduction annual flux change (mm) for the 50% biomass-reduction scenario averaged over all watersheds. Each point represents one water year. Blue line shows the calculated linear relation, and the shaded gray signifies the 95% uncertainty intervals.
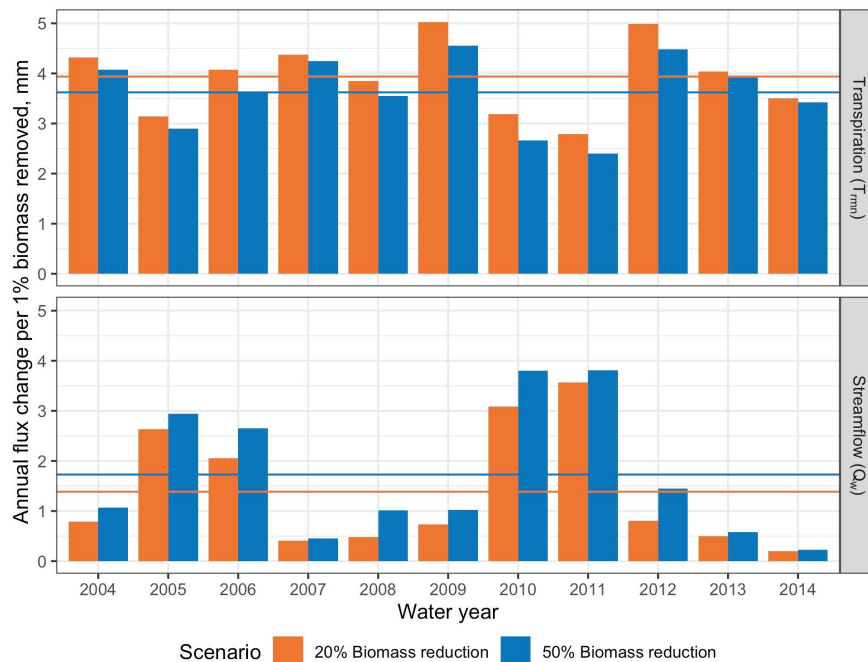

Figure 6: Increase in annual streamflow and transpiration flux from the remaining vegetation per 1% biomass removed increment for 20% and 50% biomass-reduction scenarios averaged over all watersheds. Horizontal lines indicate the mean annual flux change across all water years.
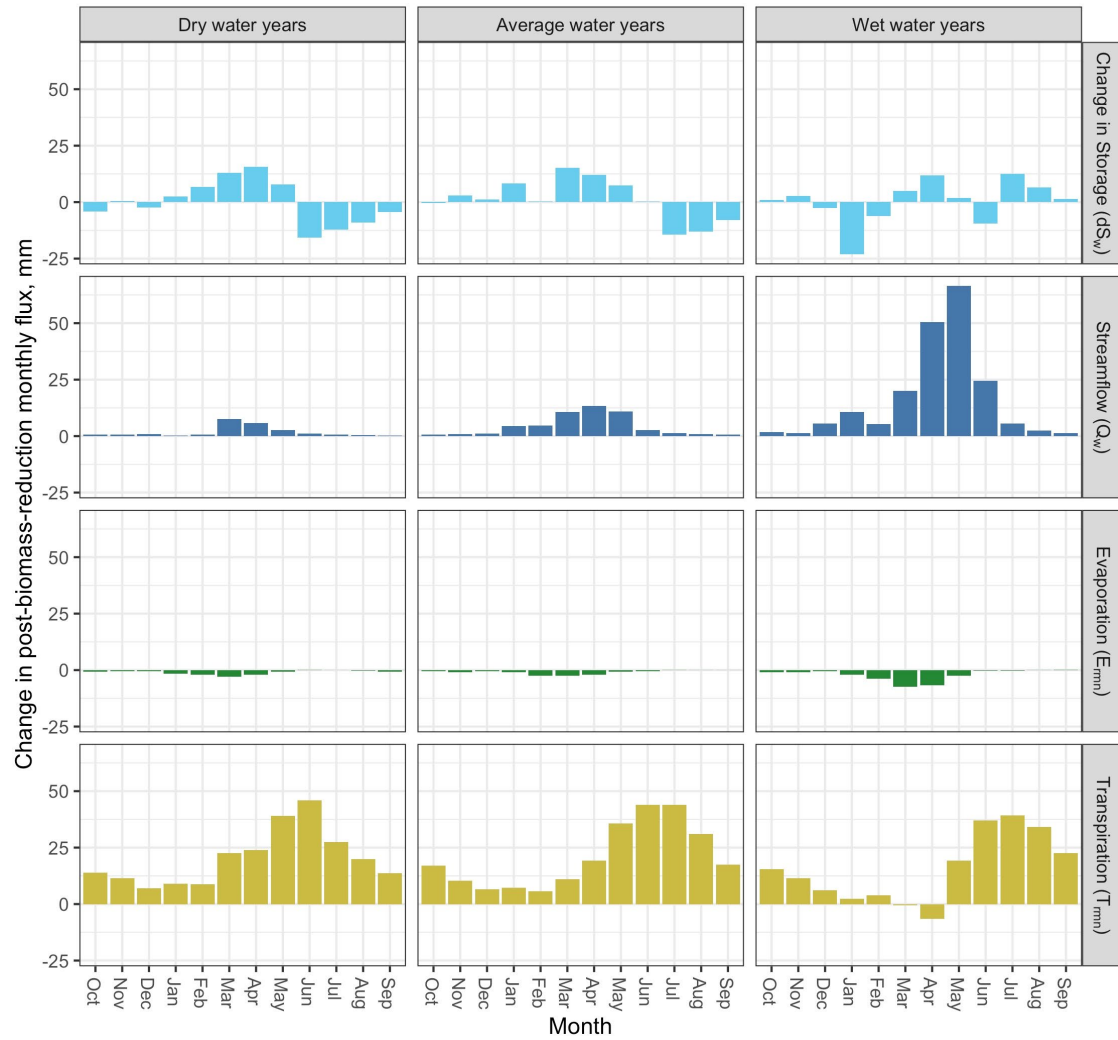
Figure 7: Change in mean monthly post-biomass-reduction storage, streamflow, evaporation, and transpiration; averaged for the three driest, four average, and four wettest water years in the P303 watershed for the 50% biomass-reduction scenario.
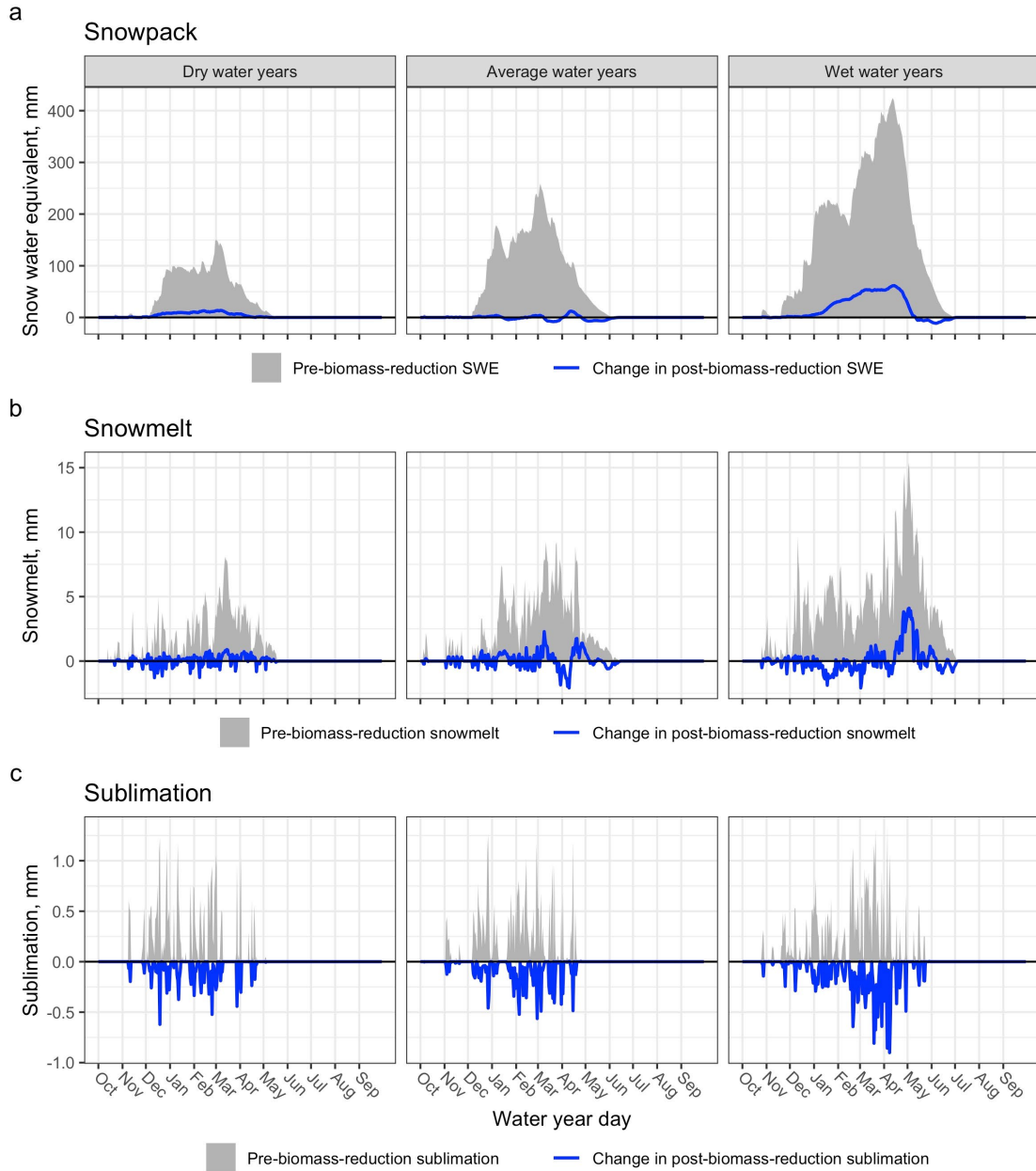
Figure 8: Mean daily pre-biomass-reduction a) snow water equivalent (SWE), b) snowmelt, and c) sublimation, as well as changes in the respective post-biomass-reduction quantities averaged for the three driest, four average, and four wettest water years in the P303 watershed for the 50% biomass-reduction scenario.

Supplemental material for

Bart RR, Ray RL, Conklin MH, Safeeq M, Saksa PC, Tague CL, Bales RC. Assessing the effects of forest biomass reductions on forest health and streamflow.

Supplemental methods: RHESSys model

Hydrologic fluxes in RHESSys are modeled from the top of the canopy to groundwater. Rainfall and snowfall may be intercepted by the canopy and litter based on vegetation size and functional type. Snowpack accumulation (both ground and canopy) was based on precipitation phases of snow and rain that were input into the model separately. Snowmelt (q_{melt}) is based on a quasi-energy budget model that incorporates radiation (M_{rad}), temperature (Mt), and advection (M_V). Snowmelt from the latter two mechanisms only occurs when the snowpack is isothermal and does not have an energy deficit, which is approximated based on a running accumulation of air temperature. Snowpack loss due to radiation (M_{rad}) in the form of sublimation, however, may occur when the snowpack has an energy deficit. Radiation-driven snow melt is a function of shortwave direct, shortwave diffuse, and local longwave radiation. Snowpack absorption of shortwave radiation is calculated based on a Beer's law extinction model through the vegetation canopy. Snowpack absorption of longwave radiation is based on air temperature (Croley, 1989). Snowmelt due to temperature (latent and sensible heat flux) is based on an empirical temperature relation that is modified by canopy fraction, while snowmelt due to advection is based on precipitation throughfall to the snowpack (see Tague and Band (2004) section 4.6 for full snowpack details).

Infiltration to the soil is based on Philip's equation (Philip, 1957) and soil water storage is conceptually divided into rooting, unsaturated, and saturated stores. Drainage from the rooting and unsaturated zone to the saturated zone is limited by field capacity, while capillary flow supports soil evaporation. Shallow-subsurface lateral drainage follows hillslope topography, with flow rates determined by water-table depth and subsurface-drainage parameters. Redistribution of subsurface water can allow down-slope vegetation to access non-local water, although access depends on rooting depth. Any surface-water flow from infiltration and saturation excess is also routed based on surface topography. A proportion of infiltrated water contributes to a deeper-groundwater linear-reservoir model that can be routed to the stream as baseflow or used to account for watershed subsurface losses.

Radiation in RHESSys is calculated based on latitude, aspect, and atmospheric variables using the MT-CLIM model (Running et al., 1987) and is attenuated through each canopy layer to the surface. Evaporation and transpiration are derived using Penman-Monteith (Monteith, 1965). Aerodynamic conductance is a function of vegetation height and based on a model developed by Haddeland and Lettenmaier (1995). The use of the Penman-Monteith equation means that transpiration responds to available radiation, vapor-pressure deficit, wind speed, and rooting-zone soil moisture through stomatal conductance. Stomatal conductance is computed using the Jarvis model (Jarvis, 1976). Greater details of the RHESSys version used in this study can be found in Saksa et al. (2017).

Supplemental methods: Model calibration

Calibration of RHESSys was separated into two components. Six subsurface flow and soil-storage parameters were quantitatively calibrated to daily streamflow using a Monte Carlo approach with 500 random parameter sets. The six parameters were hydraulic conductivity at the surface (k), decay of hydraulic conductivity with depth (m), the pore-size index (po), air-entry pressure (pa), fraction of recharge that bypasses shallow subsurface groundwater to deep groundwater stores ($gw1$), and deep groundwater flow rate to the stream ($gw2$) (Table 2). Initial ranges were selected to be broad and encompass the plausible values for each parameter. The modeled streamflow was compared to observed data that were measured from dual Parshall Montana flumes in each of the watersheds (Hunsaker & Safeeq, 2017). Many of the Providence watersheds are understood to have subsurface losses that are not accounted for by the stream gauge (Son et al., 2016). In P301 and P303, the $gw2$ parameter was set at 0, similar to the parameterization by Son et al. (2016), as this value in RHESSys directs deep groundwater out of the watershed as subsurface losses (Table 2). In P304, the

parameter was calibrated to allow discharge of groundwater to streamflow since P304 has higher sustained baseflow than P301 and P303. Three parameters affecting snowmelt; specific leaf area (*SLA*), a snow melt temperature coefficient (*SMTc*), and a radiation melt coefficient (β_{Mrad}); were calibrated to observed snow water equivalent (SWE) (Table 2). Snow water equivalent was obtained from a snow pillow at the upper Providence meteorological station (Bales et al., 2018). Since snow water equivalent was observed only at a point scale, we calibrated snow water equivalent in RHESSys using the individual patch in the model that overlays the snow pillow. This patch within RHESSys was the only patch-level output exported during calibration.

References

Bales, R., Stacy, E., Safeeq, M., Meng, X., Meadows, M., Oroza, C., Conklin, M., Glaser, S., & Wagenbrenner, J. (2018). Spatially distributed water-balance and meteorological data from the rain–snow transition, southern Sierra Nevada, California. *Earth System Science Data*, *10*(4), 1795–1805. https://doi.org/10.5194/essd-10-1795-2018

Croley, T. E. (1989). Verifiable evaporation modeling on the Laurentian Great Lakes. *Water Resources Research*, *25*(5), 781–792. https://doi.org/10.1029/WR025i005p00781

Haddeland, I., & Lettenmaier, D. P. (1995). *Hydrologic Modeling of Boreal Forest Ecosystems* (Water Resources Series 14). University of Washington. http://ntrs.nasa.gov/search.jsp?R=19980009077

Hunsaker, C. T., & Safeeq, M. (2017). *Kings River Experimental Watersheds stream discharge* [Fort Collins, CO: Forest Service Research Data Archive.]. https://doi.org/10.2737/RDS-2017-0037

Jarvis, P. G. (1976). The interpretation of the variations in leaf water potential and stomatal conductance found in canopies in the field. *Philosophical Transactions of the Royal Society of London B: Biological Sciences*, *273*(927), 593–610.

Monteith, J. L. (1965). Evaporation and environment. *Symp. Soc. Exp. Biol*, *19*, 205–234.

Philip, J. R. (1957). The theory of infiltration: 4. Sorptivity and algebraic infiltration equations. *Soil Science*, *84*(3), 257–264.

Running, S. W., Nemani, R. R., & Hungerford, R. D. (1987). Extrapolation of synoptic meteorological data in mountainous terrain and its use for simulating forest evapotranspiration and photosynthesis. *Canadian Journal of Forest Research*, *17*(6), 472–483. https://doi.org/10.1139/x87-081

Saksa, P. C., Conklin, M. H., Battles, J. J., Tague, C. L., & Bales, R. C. (2017). Forest thinning impacts on the water balance of Sierra Nevada mixed-conifer headwater basins. *Water Resources Research*, *53*(7), 5364–5381. https://doi.org/10.1002/2016WR019240

Son, K., Tague, C., & Hunsaker, C. (2016). Effects of Model Spatial Resolution on Ecohydrologic Predictions and Their Sensitivity to Inter-Annual Climate Variability. *Water*, *8*(8), 321. https://doi.org/10.3390/w8080321

Tague, C. L., & Band, L. E. (2004). RHESSys: Regional Hydro-Ecologic Simulation System—An Object-Oriented Approach to Spatially Distributed Modeling of Carbon, Water, and Nutrient Cycling. *Earth Interactions*, *8*(19), 1–42. https://doi.org/10.1175/1087-3562(2004)8<1:RRHSSO>2.0.CO;2